Chemical ordering and kinetic roughening at metal-electrolyte interfaces

P. Córdoba-Torres*
Departamento de Física Matemática y Fluidos, UNED, c/Senda del Rey 9, 28040 Madrid, Spain
(Received 19 July 2006; revised manuscript received 21 November 2006; published 7 March 2007)

In spite of the intense effort devoted in the last few years to understanding the complex dynamics of the different (electro-)chemical and physical mechanisms that take part in the metallic dissolution process, the influence of the dissolution reactive mechanism on the surface dynamics is still an open question. We present the results obtained from simulations of a microscopic metal-electrolyte interface model. The model considers a single-crystal metal that dissolves according to a reactive scheme with intermediate adsorbed species. Simulations show that roughness development induces a direct relationship between the spatial and temporal scales of the model. As a consequence of that, the time ordering of the chemical species intrinsic to the dissolution mechanism is projected spatially, leading to an unexpected chemical ordering on the interface. We show how this self-organization depends on the overall reaction kinetics and that it can be modeled from the standard macroscopic approach. One of the main consequences of the chemical ordering is that dissolution is no longer random. The heterogeneous distribution of dissolution active sites gives rise to active dissolution domains on the surface, resulting in different degrees of roughness with respect to the random dissolution reference model. These morphological differences persist in all scales. An important consequence of such complex behavior is that surface morphology changes when the electrode potential is varied during driven electrochemical dissolution. This is a remarkable result if we take into account the fact that the proposed interface model evolves under very simple conditions, namely, surface reaction kinetic control and reactivity not dependent on the local or global surface structure. Therefore, the results presented in this paper contribute to the description of metal-electrolyte interface structure and to the understanding of the processes that participate in the surface roughening observed during driven metal dissolution.

DOI: 10.1103/PhysRevB.75.115405 PACS number(s): 82.45.Jn, 82.40.Np, 68.43.−h, 82.20.Wt

I. INTRODUCTION

It is a well-known fact that self-organization can arise from the stochastic dynamics of disordered systems.[1] Dynamic evolution can lead the system toward a self-organized critical state with long-range spatial correlations characterizing these far-from-equilibrium stationary states. Within the context of reactive processes on surfaces, self-organization arises fundamentally as a consequence of the interplay between the dimensional restriction to the reaction imposed by the boundary conditions—reactive process is bounded to the substrate or interface—and the participation of irreversible nonlinear reactive mechanisms.[2] Effects such as aggregation of one species or segregation between two species are, in many cases, due to lateral interactions among adsorbates[3–5] and/or to nonrandom adsorption mechanisms.[6–8] In the case of alloys, for instance, segregation between two elements in binary alloys[9] or cosegregation between two or many elements in multialloys[10] seems to be directly related with the surface enrichment induced by the adsorption of some species,[11] giving rise to the formation of adsorbate structures.[12] Another important cause for spatial heterogeneity is the restriction to the reactant diffusion imposed by a low dimensionality of the support or due to a sufficiently low temperature. In the case of reactive processes involving nonlinear reactions,[13–15] the reactive mechanism itself induces a heterogeneous distribution of reactants, even in the case of noninteracting adsorbates, a diffusion-limited reaction, and the presence of random adsorption mechanisms.[16] In almost all cases, surface self-organization dramatically affects reaction kinetics[17–19] and surface morphology.[20–23] Therefore, the study of mechanisms that can lead to self-organization becomes crucial in growth processes[24] as well as in several heterogeneous chemistry domains such as catalysis (see Refs. 25–28 for the case of catalytic activated reactions), oxidation,[29] adsorption,[12] or corrosion.[30]

Within the context of the electrochemical processes of metal dissolution, preliminary results obtained from computer simulations of a metal-electrolyte interface model evolving under open-circuit potential conditions showed an unexpected reactant self-organization at the interface.[31] This kinetic-induced heterogeneity was unexpected since the model did not consider any of the classical mechanisms that may induce chemical ordering: dissolution kinetics was under surface reaction control (ion diffusion from and/or into the electrolyte was supposed to be much faster than charge-transfer reactions, so Laplacian fields around surface are not considered); all the reactions conforming to the reactive mechanism of dissolution were linear; reactivity was independent of the surface position; neither interaction between adsorbates, preferential adsorption-desorption mechanisms, nor passivation processes were considered; the electrolyte composition was assumed perfectly uniform and the metallic electrode was considered as a perfect monocrystal without defects. Even for so simple an interface model, evidence pointed to a chemical ordering resulting from the interplay between the reactive kinetics and the surface roughness. In the first part of this paper, we present a different mechanism of surface chemical ordering that accounts for those results and we describe its most important features.

This self-organization has important consequences on the interface evolution. In the second part of this work, we analyze one of them: its influence on the dynamics of surface

roughness. As we shall see, one of the most important effects of the chemical ordering is that dissolution is no longer spatially random, but it occurs mainly at those positions occupied by the heterogeneously distributed dissolution active sites, thus giving rise to surface domains where dissolution takes place. As the chemical self-organization is reaction kinetics dependent, changes in the kinetics—due to variations in the driven force for dissolution, as the applied electrical potential, for instance—lead to changes in the surface roughness. The results presented in this paper thus represent a contribution to the understanding of the surface roughening observed during driven metal dissolution in aqueous solutions.

The link between an external parameter such as the potential and surface topography is a very important issue in surface electrochemistry.[32–34] The wide research in the metal dissolution mechanisms has shown that at low currents, when the dissolution rate is controlled by surface processes involving mainly interfacial charge-transfer reactions, dissolution occurs principally at those surface active sites weakly bonded to the surface[35]—as kinks in the steps on the crystal surface.[36] This establishes a direct link between surface roughness and dissolution rates—rough surfaces exhibit more low-coordinated sites and, consequently, show higher dissolution rates. Changes in the roughness induced by the varying applied potential may lead to changes in the dissolution mechanism, thus having a considerable influence on the overall reaction as has been reported by some models.[37] In the anodic dissolution of iron, for instance, electrochemical surface roughening has been observed experimentally,[38,39] showing an increasing number of kinks, where dissolution mainly takes place, as the anodic potential increases. In acid solutions, the Cu electrodissolution also proceeds predominantly from kinks,[40] Cu(100), or step edges,[41] Cu(111), with rates of dissolution increasing as the potential was increased.

Many models have been proposed to explain the variation of roughness with the electrode potential. Most of them have tried to discern the dominant physical process without addressing the electrochemical aspects of the problem. Furthermore, they have only addressed specific cases, thus resulting excessively ad hoc and phenomenological. By comparing *in situ* sequential scanning tunneling microscope imaging of roughness evolution during the electrodissolution of Ag with general nonelectrochemical atomistic and continuum models derived in the framework of the dynamic scaling theory,[42,43] Vela *et al.*[44] explained that the increase in roughness of the Ag single-crystal surface from low to high current densities was due to the atom surface diffusion with energy barriers at step edges. In the case of anodic dissolution of Cu in acid solutions with potentials assuring a process under a surface reaction kinetic control, nanoscopy imaging[45–48] revealed again a different roughening behavior: in null current conditions, the Cu surface processes—principally the surface mobility of Cu atoms—lead to a smoothening of small pits, while for constant current densities, an inhomogeneous attack proceeds, resulting in different surface domains that obey different dissolution models, one of them favoring deep pit growth and thus turning the interface unstable. Discrete[45,49] and continuum[48] models, in which surface processes are influenced by the development of unstable singularities induced by nonlocal effects (electrodissolution enhancement at tip cavities), were proposed to account for the experimental observations. Driven morphological instabilities have also been observed during anodic dissolution of sputter-deposited nickel films.[50] Influence of potential on the roughness regime becomes crucial in the anodic dissolution of alloys. In the dealloying of brass,[51] for instance, under potentials favoring the electrodissolution of zinc and the formation of vacancies and copper islands, evolving alloy interface displays two consecutive different roughness regimes: a first one, which exhibits a stable interface controlled by surface diffusion and second one in which a negative surface tension effect that enhances zinc electrodissolution at cavities turns the interface unstable.

In some cases, an explanation of the heterogeneous dissolution induced by the applied electrochemical potential and its influence on the surface topography development has been qualitatively attempted in terms of the possible reaction mechanism taking place at the interface, as in the Cu electrodissolution.[45] In spite of these efforts, the influence of the adsorption-desorption processes at the electrode surface has been assumed negligible or simply not considered in most theoretical models, although this effect has been observed experimentally.[41,47,52] As far as we know, no exhaustive analysis of the interplay between surface dynamics and electrochemical kinetics has been done, and modeling of the dissolution reactive mechanism has thus generally considered its simplest and often multielectronic one-step form: $M \xrightarrow{k} M_{\mathrm{sol}}^{z+} + ze^-$, where sol denotes the M ionic species at the electrolyte solution and the kinetic constant k can depend on the local coordination (surface site reactivity dependent on the local surface structure).[37,43,49,53,54] However, in general, dissolution reaction follows electrochemical reactive mechanisms that must consider several dissolution routes and usually involve intermediate reaction steps, yielding intermediate metallic species associated with adsorption-desorption processes of ions from the electrolyte. Their spatial distribution and influence on the surface dynamics are explored in this work.

II. CHEMICAL ORDERING MECHANISM

A. Reactive and computational model

A metal dissolution process may actually be modeled with the help of a branched scheme of alternative routes, each of them composed of a succession of electron exchange reactions. In each of these paths, the metal atom evolves through a cascade of intermediate compounds formed in combination with ions present in the electrolyte. A single linear chain of reactions is the simplest of such models:

$$M(0) \underset{k_{-1}}{\overset{k_1}{\rightleftarrows}} M(\mathrm{I})_{\mathrm{ads}} \underset{k_{-2}}{\overset{k_2}{\rightleftarrows}} M(\mathrm{II})_{\mathrm{ads}} \underset{k_{-3}}{\overset{k_3}{\rightleftarrows}} \cdots M(n)_{\mathrm{ads}} \xrightarrow{k_{n+1}} \phi(\mathrm{solution}). \tag{1}$$

Here, the original metal atom—state $M(0)$—jumps from left to right progressively, assuming more oxidized forms that combine into adsorbates, $M(i)_{\mathrm{ads}}$, and finally ending up irreversibly into the electrolyte. There are two solid reasons for focusing on such a model. First, despite its simplicity, the sequential pattern in Eq. (1) is the basic building block of more realistic approaches in the understanding of metal dissolution processes. As a matter of fact, dissolution models proposed in the literature display reactive schemes that differ in complexity. In Ref. 55, for instance, a reaction model is proposed to account for the stationary—steady-state polarization curve—and transient—electrochemical impedance—responses of iron electrodes in acidic medium. The model considers three dissolution paths and includes three adsorbed reaction intermediate species. It can be seen that each dissolution route is given by Eq. (1) with $n=1$ and $n=2$.

In second place, model (1) also displays unambiguously the self-ordering features at the root of the chemical and morphological heterogeneities associated with the surface roughening we shall show in this paper. In order to display the general features of concern to the present work, we shall address a particular case of Eq. (1): the three-adsorbate case, with intermediate states $M(\mathrm{I})_{\mathrm{ads}}$, $M(\mathrm{II})_{\mathrm{ads}}$, and $M(\mathrm{III})_{\mathrm{ads}}$.

The working interface model is similar to that already presented,[31] so we only enumerate its principal hypotheses. (1) All adsorbates obey the Langmuir isotherm—no lateral interactions are allowed—and consequently form monolayers. (2) Kinetic regime is limited by charge-transfer reactions—mass transport across the interface from and/or into the electrolyte is much faster than charge-transfer processes. (3) Chemical and electric potentials are independent of the local structure—reactivity of chemical species does not depend on their position on the interface. (4) Surface diffusion is frozen, so no surface relaxation occurs via this process (far-from-equilibrium evolution condition). These assumptions are rather restrictive and unrealistic but they allow a complete assessment of the consequences of the kinetically induced chemical ordering inherent to the model. Monte Carlo simulations of the interface evolution have been carried on a $(1+1)$-dimensional $[(1+1)\mathrm{D}]$ lattice representing a perfect monocrystal with a metal atom as the lattice unit. Dissolution process is simulated by assigning a cellular state to each chemical species and a transition rule to each elemental step of the dissolution reactive mechanism. These transition rules are governed by transition probabilities R_i directly related with the corresponding kinetic constants: $\{R_i\}=b\{k_i\}$ (results are independent of the rescaling factor b). Different geometries and different neighborhoods (Von Neumann, four first neighbors in a square lattice; Moore, eight first neighbors in a square lattice and six first neighbors in a triangular lattice) have been considered and no qualitative differences have been observed in the results. The lattice is initially set in state $M(0)$, representing the metal electrode, except for the uppermost row, which is in state ϕ in the representation of the electrolyte. The initial interface is perfectly flat. Once the dissolution process starts, the hitherto plane interface roughens and evolves by defining a preferential direction of growth along the vertical axis. The lattice width L, which has been varied between 10^2 and 2×10^4 units, represents the mesoscopic scale of the model ($\sim\mu$m), while we shall refer to the limit $L\to\infty$ as the macroscopic scale.

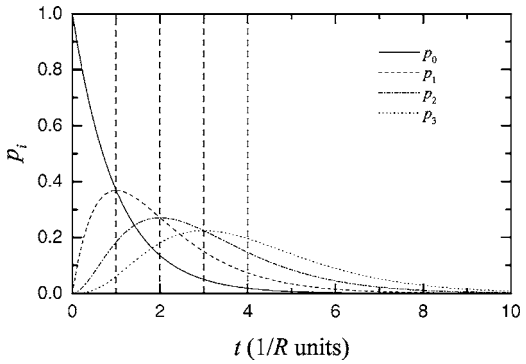

FIG. 1. Time evolution (in $1/R$ units) of p_i obtained by solving Eq. (2) in the case $R_i=R$ and $R_{-i}=0$. The vertical broken lines correspond to the mean times $\tilde{t}_i$ calculated from Eq. (4).

B. Chemical ordering and surface roughening

From a statistical point of view, the reactive mechanism establishes a chronology in the occupation of the accessible states. In order to formalize this idea, we can imagine a closed set of N particles initially in state $M(0)$ and let the ensemble evolve according to the rules define by Eq. (1) and particularized to the three-adsorbate case. In the thermodynamic limit $N\to\infty$, the probabilities p_i, $i=0,\ldots,3$, of finding a site in any of the states $M(i)$ at any time t follows the set of differential equations below:

$$\frac{d}{dt}p_0 = p_1R_{-1} - p_0R_1,$$

$$\frac{d}{dt}p_1 = p_0R_1 + p_2R_{-2} - p_1(R_{-1}+R_2), \tag{2}$$

$$\frac{d}{dt}p_2 = p_1R_2 + p_3R_{-3} - p_2(R_{-2}+R_3),$$

$$\frac{d}{dt}p_3 = p_2R_3 - p_3(R_{-3}+R_4).$$

The initial conditions are $p_0(t=0)=1$ and $p_i(t=0)=0$, for $i=1,2,3$. From Eq. (2), we have

$$\frac{d}{dt}\sum_{i=0}^{3} p_i = -p_3R_4, \tag{3}$$

from which we obtain $\Sigma_{i=0}^{3}p_i<1$, for $t>0$. This is obvious if we take into account that the probabilities p_i in Eq. (2) represent fractions of the initial set N and the system evolves toward the complete dissolution: $p_i(\infty)=0$.

Figure 1 illustrates an example of sequential state occupation by presenting the following solutions to Eq. (2) in the case of uniform forward ($R_i=R$) and zero backward elementary transition rates ($R_{-i}=0$): $p_0(t)=e^{-Rt}$, $p_1(t)=Rte^{-Rt}$, $p_2(t)$

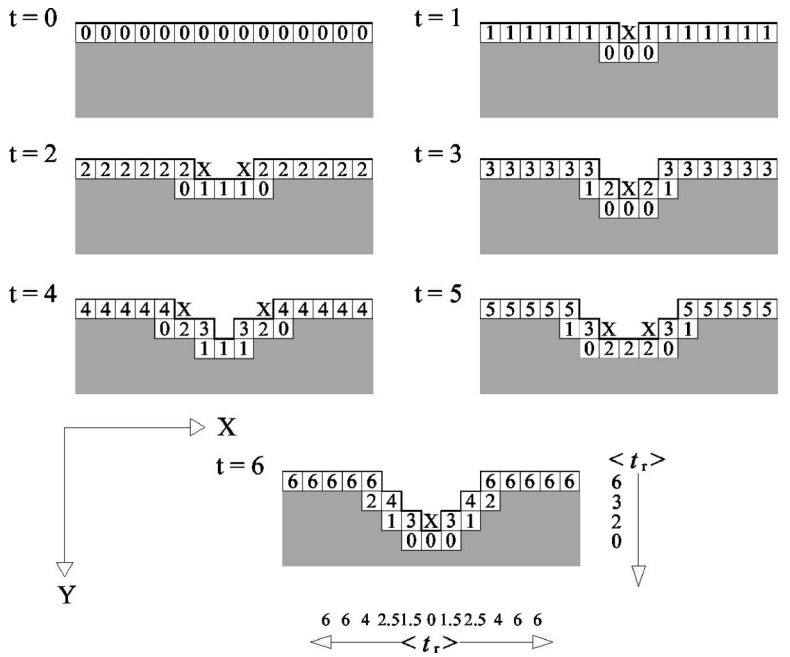

FIG. 2. Illustration of the evolution of a microscopic perturbation in the corrosion front. As the dissolution proceeds, the morphological perturbation propagates into the metallic bulk, yielding roughness. For the sake of simplification, we have assumed the simpler dissolution mechanism $M \xrightarrow{R} M_{\mathrm{sol}}^{z+} + ze^-$ with a small reaction probability ($R \approx 1/L$), so only one or two cells may dissolve in each Monte Carlo step. Residence time t_r in Monte Carlo units has been indicated inside those metallic cells belonging to the interface (according to the Monte Carlo algorithm, all surface sites have been visited, on average, once in each unit of time or MC step). The crosses stand for the just dissolved cells. The thick line represents the metallic surface profile, which is initially ($t=0$) flat. After six MC steps, the evolution of the morphological perturbation has generated spatial correlations among the average residence times of interface cells, $\langle t_r \rangle$, both in the propagation (Y) and in the horizontal (X) direction. Moore neighborhood has been considered. Symmetry in both sides of the indentation with respect to height is only significant from a statistical point of view.

$=(Rt)^2 e^{-Rt}/2$, and $p_3(t)=(Rt)^3 e^{-Rt}/6$. It can be seen that dissolution evolves through different stages, in which increasing oxidation level species are sequentially preponderant. The broken vertical lines indicate the value of the mean time of occurrence of each stage in the dissolution mechanism, evaluated according to

$$\tilde{t}_i = \frac{\int_0^\infty p_i(t) t dt}{\int_0^\infty p_i(t) dt}, \quad i = 0, \ldots, 3. \tag{4}$$

Solving Eq. (4) for the case displayed in Fig. 1 yields $\tilde{t}_i=(i+1)/R$, implying $\tilde{t}_i < \tilde{t}_{i+1}$ for $i=0,1,2$. This time ordering in state occupation is actually a general feature of Eq. (1). In the general case of nonuniform forward and backward transition probabilities, values of $\tilde{t}_i$ depend in a complex form on the whole set of reaction probabilities, but in any case, mean times corresponding to different species are always different and increasing in the $0 \rightarrow 3$ oxidation level direction, which proves that there is a time ordering of species implicit into the reactive scheme.

The above specific sequence of stages in the dissolution route has an important consequence as far as the surface distribution of adsorbates and the surface roughening is concerned. Figure 2 shows how the evolution of a local indentation into the metal bulk carries a time-differentiation process along the direction of penetration. Evolution is associated with the sequential incorporation of new lattice sites into the interface as a result of the dissolution process. Each cell in the figure is characterized by the number of time steps (times it has been visited by the Monte Carlo algorithm) elapsed since it has become part of the interface, i.e., exposed to the chemical action of the electrolyte. We call it residence time t_r. As the notch grows into the metal bulk, cells newly uncovered are preferably located at the bottom of the pit, while its upper rim is constituted of older interface cells. Averages for t_r taken along lattice rows and columns after six steps indicate a sequential dating of interface cells along the sides of the etch.

Following the discussion of Figs. 1 and 2, a link may then be established between position and residence time of interface cells, and consequently between position and state occupancy in the reaction chain (1). Figure 3 illustrates that fact for the kinetic case of Fig. 1. Average residence time corresponding to height h, $\langle t_r \rangle(h)$, appears at the bottom of the figure, where height h is defined for each position as the distance along the vertical direction from the lowermost interface site. Starting from the bottom of the indentation, the first sector, with $0 \leqslant \langle t_r \rangle < 1/R$, will consist of cells more likely in state $M(0)$ (see Fig. 1); the second sector, with $1/R < \langle t_r \rangle < 2/R$, will consist mostly of cells in state $M(\mathrm{I})_{\mathrm{ads}}$, while the third and fourth sectors, with $2/R < \langle t_r \rangle < 3/R$ and

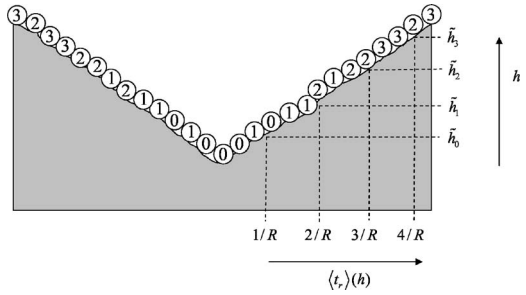

FIG. 3. Illustration of the microscopic chemical ordering. The balls represent the chemical species covering totally the surface of an indentation into the metallic bulk (in gray). The numbers inside the balls correspond to the oxidation state in the reaction chain (1). The broken horizontal lines indicate the mean height of each species, $\tilde{h}_i$, defined in Eq. (5), while the broken vertical lines point out interface positions with average residence times equal to $\tilde{t}_i$. Both positions coincide (horizontal and vertical dotted lines intersect at surface positions) because we have assumed a linear relationship for $\langle t_r\rangle_i(h)$. Symmetry in both sides of the indentation with respect to height is only significant from a statistical point of view.

$\langle t_r\rangle > 3/R$, respectively, will be predominantly made up of cells in states $M(\mathrm{II})_{\mathrm{ads}}$ and $M(\mathrm{III})_{\mathrm{ads}}$, in that order. In this way, a microscopic chemical ordering emerges along the interface of surface indentations during the roughening process.

The spontaneous organization illustrated in Fig. 3 becomes apparent in both the microscopic and the mesoscopic scales of the model and survives into the stationary regime, attained after a time T^* of simulation when the chemical and morphological parameters saturate to a constant mean value. From a microscopic point of view, the chemical ordering will result in nontrivial correlations among the chemical species that show a surface distribution of reactants, in which cells in the same state are most likely to be closer, while consecutive states in the dissolution path will frequently appear as neighbors on the interface. On the mesoscopic level, a stationary ordering of the species will appear in the direction of propagation of the corrosion front, as illustrated in Fig. 3, where the mean height of each state $\tilde{h}_i$, defined below, has been indicated in the right side. With the term stationary we mean that this ordering persists in time once the stationary is reached (snapshots of interface taken at different times will display the same mesoscopic ordering).

By denoting as $\vartheta_i(t,h)$ the probability of finding a cell in state i at residence time t and height h, the average residence time of cells in state i as function of height, $\langle t_r\rangle_i(h)$, and the mean height $\tilde{h}_i$ are defined as follows:

$$\langle t_r\rangle_i(h) = \frac{\int_t t\vartheta_i(t,h)}{\int_t \vartheta_i(t,h)}, \quad \tilde{h}_i = \frac{\int_h h\int_t \vartheta_i(t,h)}{\int_h\int_t \vartheta_i(t,h)}. \tag{5}$$

It must be noticed that the residence time associated with each species encompasses the whole lifetime of a cell, from the moment it first belonged to the interface (forcibly in state M) until the running time. This means, for instance, that the residence time of a cell in state $M(\mathrm{I})_{\mathrm{ads}}$ incorporates the time it spent in state M before jumping to $M(\mathrm{I})_{\mathrm{ads}}$.

According to Eq. (5), if the function $\langle t_r\rangle_i(h)$ is linear, i.e., the average residence time associated with each state increases linearly with height, we then have $\tilde{t}_i = \langle t_r\rangle_i(\tilde{h}_i)$. That means that the interface position with height $\tilde{h}_i$ has an average residence time for state i exactly equal to $\tilde{t}_i$. This fact has been represented in Fig. 3 with the horizontal and vertical broken lines.

C. Simulation and results

The results obtained from the model simulations support the ideas developed in the previous section. The normalized distribution of the residence times associated with each state, obtained from the analysis of a large number of interfaces during a simulation of the three-adsorbate case with $R_i = R$ and $R_{-i} = 0$, agrees perfectly with the theoretical ones displayed in Fig. 1. In Fig. 4, we depict the normalized pair-correlation functions obtained in the same simulation and defined as

$$\Gamma_{ij}(r,t) = \frac{\langle \sigma_i(\mathbf{r}_1,t)\sigma_j(\mathbf{r}_2,t)\rangle}{\Theta_i(t)\Theta_j(t)}, \tag{6}$$

where the bracket $\langle\cdot\rangle$ indicates spatial averaging over the interface. The microscopic density $\sigma_i(\mathbf{r},t)$ takes the value of 1 if, at time t, the cell at position $\mathbf{r}$ is in state $M(i)$, while $\sigma_i(\mathbf{r},t)=0$ otherwise; $\Theta_i(t)$ is the surface coverage fraction of species $M(i)$, equal to $\langle\sigma_i(\mathbf{r},t)\rangle$; and r is the distance (in lattice units) between positions $\mathbf{r}_1$ and $\mathbf{r}_2$. This distance is given by the shortest path along the surface and is different from the Euclidean distance $|\mathbf{r}_1-\mathbf{r}_2|$ on rough surfaces. Values for $\bar{\Gamma}_{ij}(r) = \langle\Gamma_{ij}(r,t)\rangle_{t>T^*}$ in the figures are the result of time averages once the stationary is reached ($t > T^*$).

Figure 4(a) shows the spatial decay of correlations for cells in the same state ($i=j$). The results show positive correlations at first neighbors for all states [$\bar{\Gamma}_{ii}(1) > 1$]. This value and the degree of packing decrease as we go across the dissolution path from left to right. Figure 4(b) displays correlations between consecutive states ($j=i+1$). The decay of $\bar{\Gamma}_{01}(r)$ indicates that states $M(0)$ and $M(\mathrm{I})_{\mathrm{ads}}$ are neighbors. This interaction is weaker between adsorbates $M(\mathrm{I})_{\mathrm{ads}}$ and $M(\mathrm{II})_{\mathrm{ads}}$, while $\bar{\Gamma}_{23}(r)$ shows that, although cells in states $M(\mathrm{II})_{\mathrm{ads}}$ and $M(\mathrm{III})_{\mathrm{ads}}$ are neighbors too, the pairs $M(\mathrm{II})_{\mathrm{ads}} - M(\mathrm{III})_{\mathrm{ads}}$ are sparsely distributed, in agreement with the results of the previous figure. Finally, nonconsecutive states in the dissolution path are not neighbors in their distribution on the interface, as can be inferred from the negative correlations displayed in Fig. 4(c).

Differences among the correlations of different chemical species lie beneath the behavior displayed in Fig. 1. It can be inferred, for instance, that the level of packing of state M

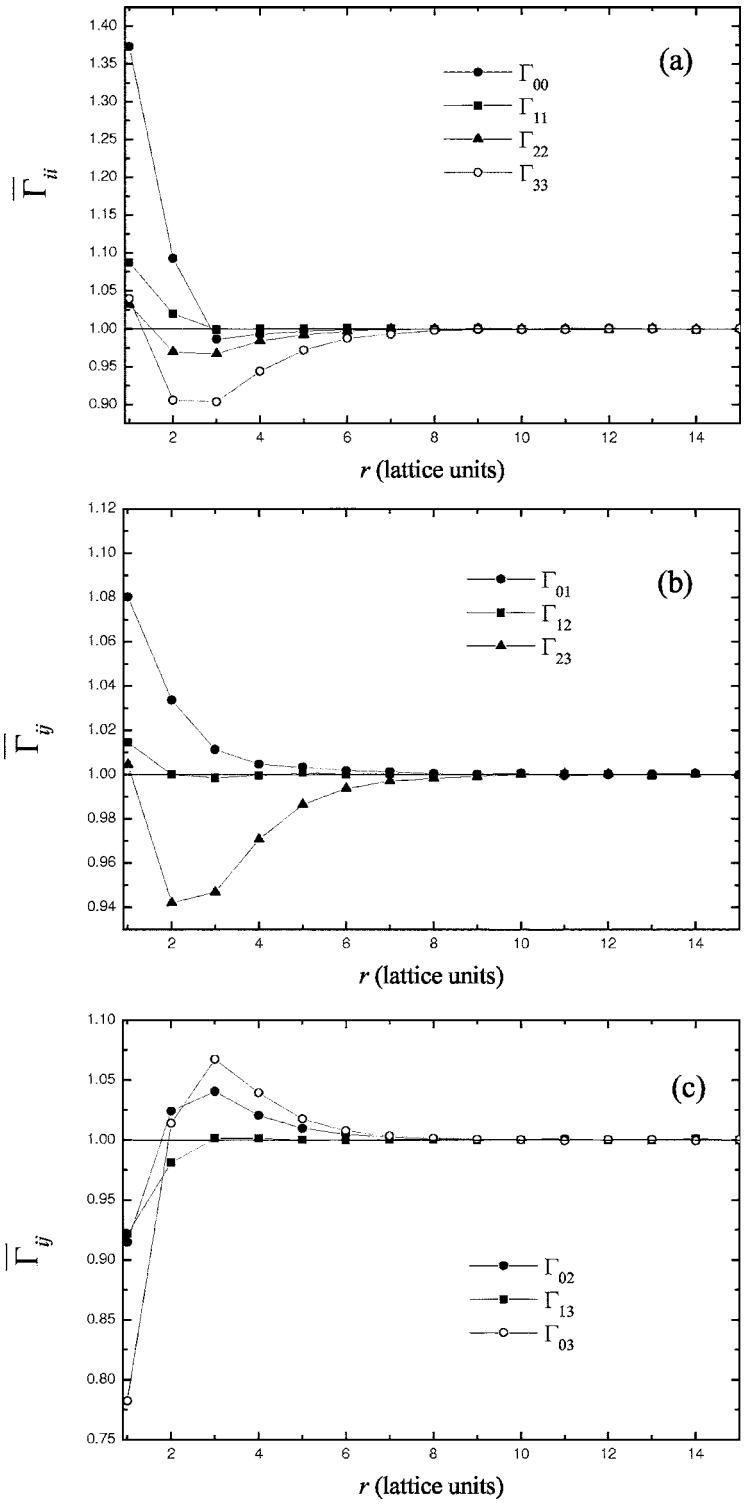

FIG. 4. Spatial decay of the pair correlation function defined in Eq. (6) obtained from a simulation of the three-adsorbate case with $R_i=R$ and $R_{-i}=0$: (a) $\bar{\Gamma}_{ii}(r)$, (b) $\bar{\Gamma}_{ii+1}(r)$, and (c) $\bar{\Gamma}_{ii+2}(r)$. Points have been joined to guide the eyes.

will be larger than that of species $M(\mathrm{I})_{\mathrm{ads}}$ since the difference between p_0 and p_1,p_2,p_3 within the interval $0 \leqslant t < \tilde{t}_0$ is much larger than the difference between p_1 and p_0,p_2,p_3 when $\tilde{t}_0 < t < \tilde{t}_1$.

Figure 5 offers a different kind of picture in order to assess the chemical ordering on the mesoscopic scale. It displays the normalized distribution of chemical species along the preferential (vertical) direction Y of interface growth,

$$N_i(h) = \left\langle \frac{n_i(t,h)}{\left(\sum_{h=0}^{h_{\max}(t)} n_i(t,h) \right)} \right\rangle_{t>T^*}, \tag{7}$$

where $n_i(t,h)$ is the number of interface cells in state $M(i)$ at time t and at height h ($h=0$ for the lowermost interface site and $h=h_{\max}$ for the highest one). The mean height of each

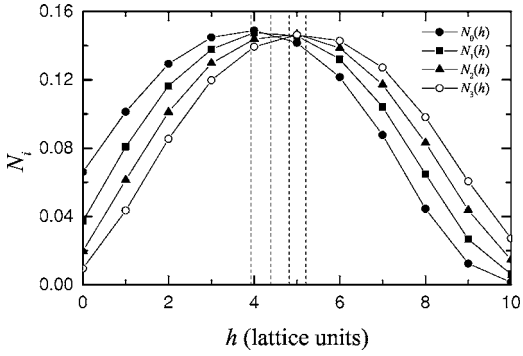

FIG. 5. Normalized height distributions of species obtained at the steady state of a simulation of the three-adsorbate case with $R_i=R$ and $R_{-i}=0$. The points have been joined to guide the eyes. The sampling has considered interfaces with $h_{\max}=10$. The lattice size was $L=100$. The mean height of species i, $\tilde{h}_i$, calculated from Eq. (8), has been indicated in the figure with a vertical broken line.

species, calculated from the discrete version of Eq. (5),

$$\tilde{h}_i = \left\langle \frac{\sum_{h=0}^{h_{\max}(t)} n_i(t,h)h}{\sum_{h=0}^{h_{\max}(t)} n_i(t,h)} \right\rangle_{t>T^*}, \tag{8}$$

has been indicated in the figure with a vertical broken line. It can be seen that microscopic chemical organization leads to a heterogeneous height distribution of species and that the resulting ordering is consistent with the position of the corresponding state in the dissolution mechanism, as predicted in Fig. 3.

In the discussion of Fig. 3, we pointed out the fact that if $\langle t_r\rangle_i$ increases linearly with height, the height interface position corresponding to $\tilde{h}_i$ has exactly an average residence time associated with state i equal to $\tilde{t}_i$. In Fig. 6, we show that the function $\langle t_r\rangle_i(h)$ obtained in the simulations, although monotonously crescent, is not linear. However, it can be seen that the hypothesis of the linear approximation holds and $\tilde{t}_i \approx \langle t_r\rangle_i(\tilde{h}_i)$. Based on that approximation, we can hope that mean times $\tilde{t}_i$ will capture, in some way, the dependence of $\tilde{h}_i$ on the reactive kinetics. This supposition will play a key role in the modeling of the driven kinetic roughening presented in the next section.

We have seen that the results displayed in Figs. 4–6 are consistent with the scenario presented in Fig. 3 for the simplest kinetic case of scheme (1). However, the characteristics of the chemical ordering presented in that scenario, both in the miscroscopic (range and intensity of correlations) and mesoscopic (type and degree of ordering) scales, depend on the electrochemical kinetics of the overall scheme: changes in the values of the set of reaction probabilities $\{R_i\}$ lead to changes in the chemical ordering. Next, we shall see that this has important consequences as far as the surface roughness is concerned.

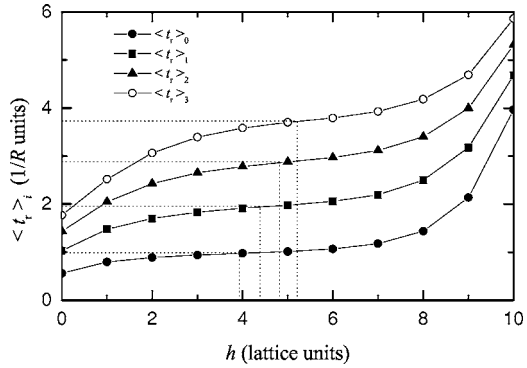

FIG. 6. Height variation of the average residence time for each state i, $\langle t_r\rangle_i(h)$, in $1/R$ units, obtained from the same simulation to that of Fig. 5. Mean heights $\tilde{h}_i$ and mean times $\tilde{t}_i$ have been indicated by vertical and horizontal dotted lines, respectively.

III. PREFERENTIAL DISSOLUTION

Dissolution takes place at interface positions occupied by the dissolution active cells, i.e., those cells in the intermediate state that leads to the dissolution elementary step [state $M(\mathrm{III})_{\mathrm{ads}}$ in the three-adsorbate model proposed above]. Therefore, if the distribution of reactants on interface is heterogeneous, dissolution will not occur randomly. We shall refer to it as preferential dissolution.

In the example of the previous section, dissolution active cells were located, on average, in the upper parts of the interface. That means that dissolution will occur principally at the top of bumps on the rough surface. Then, preferential dissolution will have an opposite effect on the development of roughness, contributing as a stabilizing mechanism in the evolution of morphological perturbations. This will lead to a degree of roughness lower than that in the random dissolution case. Now we can imagine the opposite case—not possible in the previous model—in which kinetics of the reactive scheme leads to dissolution active cells to cover the lower parts of the interface. The preferential dissolution at the surface valleys will destabilize the evolution of the morphological perturbations of the front, thus enhancing roughness. Therefore, changes in the dissolution kinetics lead to changes in the distribution of reactants on the interface, a fact that induces differences in the preferential dissolution, resulting in different levels of roughness.

A. Kinetic roughening during driven metal dissolution

One important result is that chemical and physical properties of interface are invariant under an isotropic rescaling of the kinetic parameters, $\{k_i'\}=b\{k_i\}$, which only amounts to a simple rescaling of time exclusively affecting the pace of the overall process. Only an anisotropic transformation leads to changes in the distribution of reactants and, consequently, to a different degree of irregularity. Therefore, interface features depend only on the relative values of the whole set of kinetics parameters taking part in the process. This result has important consequences regarding driven-dissolution processes, i.e., metallic dissolution processes driven by means of an externally applied potential, in which the variation of

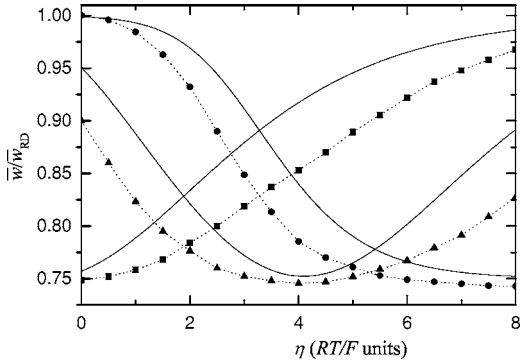

FIG. 7. Values of $\bar{w}/\bar{w}_{\mathrm{RD}}$ vs η (in RT/F units) obtained after simulations of the driven dissolution of an electrode of size $L=1000$ and triangular structure. Each set of points corresponds to a different set of kinetic parameters $\{k_{0,1}, k_{0,2}, k_{0,-1}, \alpha_1, \alpha_2\}$: points {0.0135, 0.0135, 0.369, 0.5, 0.5}; triangles {0.0082, 0.00116, 0.0045, 0.5, 0.99}; and squares {0.0068, 0.0095, 0, 0.5, 0.99}. Each point is the average of 1000 independent runs starting from a flat surface. The symbols have been joined with the broken lines to guide the eyes. The continuous lines stand for the analytic kinetic approach to each set of points given by $\tilde{t}/\tilde{t}_1$ in Eq. (18).

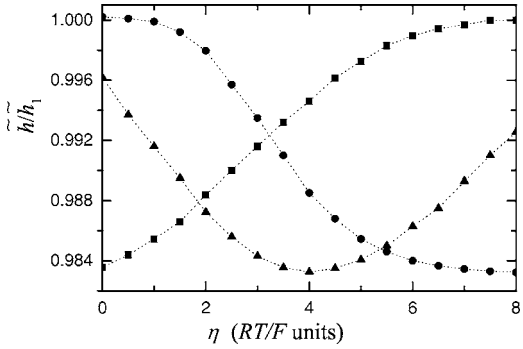

FIG. 8. Values of $\tilde{h}/\tilde{h}_1$ vs η obtained in the same simulations to those of Fig. 7. The symbols have been joined to guide the eyes.

the surface roughness with the applied potential is a well-asserted fact.

The classical nonequilibrium electrochemical kinetics determines that the energy $zF\eta$ supplied by the overpotential η (regarding the open-circuit potential) is distributed in the elementary step i in the following way: $\Delta G^*_{a,i}=\Delta G^*_{0,i} - z\alpha_i F\eta$ and $\Delta G^*_{c,-i}=\Delta G^*_{0,-i}+(1-\alpha_i)zF\eta$, where $\Delta G^*_{a,i}$ and $\Delta G^*_{c,-i}$ are the activation energies in the oxidation (forward anodic reaction) and in the reduction (inverse cathodic reaction), respectively, z is the number of electrons implied in the step, and α_i is the transfer coefficient ($0 \leqslant \alpha_i \leqslant 1$). From this hypothesis, the Tafel law is obtained for the kinetic constants k_i and k_{-i}: $k_i=k_{0,i}\exp(\alpha_i F\eta/RT)$ and $k_{-i}=k_{0,-i}\exp[-(1-\alpha_i)F\eta/RT]$, where we have considered $z=1$. In order to simulate the electrode polarization, transition probabilities of the model are then assumed in the following way:

$$R_i = R_{0,i} e^{\alpha_i (F/RT)\eta},$$

$$R_{-i} = R_{0,-i} e^{-(1-\alpha_i)(F/RT)\eta}. \tag{9}$$

Different values of the transfer coefficients entail differences in the response of the elementary transition probabilities to changes in the overpotential, thus leading to a variation in the relative kinetics among the elementary steps. Accordingly, chemical organization and surface roughness at steady-state polarization will depend on the electrode overpotential η.

We have simulated the anodic dissolution of the electrode using a simplified version of Eq. (1) that considers a single adsorbate ($n=1$). The model was proposed by Bockris[56] to explain the experimental steady-state polarization curves obtained during driven dissolution of Fe in acid environment and is given by the following reactions:

$$\begin{aligned} &\mathrm{Fe} + \mathrm{OH}^- \underset{k_{-1}}{\overset{k_1}{\rightleftarrows}} (\mathrm{FeOH})_{\mathrm{ads}} + e^-, \\ &(\mathrm{FeOH})_{\mathrm{ads}} \xrightarrow{k_2} (\mathrm{FeOH})^+_{\mathrm{sol}} + e^-. \end{aligned} \tag{10}$$

Interface roughness at time t is characterized by the interface width, given by the standard height deviation

$$w(L,t) = \sqrt{\frac{1}{L}\sum_{j=1}^{L} [h_j(t) - \langle h_j(t)\rangle]^2}, \tag{11}$$

where $h_j(t)$ is the interface height at horizontal lattice position j and $\langle h_j(t)\rangle$ is the average height: $\Sigma_{j=1}^{L} h_j(t)/L$. In order to avoid the influence of overhangs, we shall consider in Eq. (11) the minimum value of the heights for a given position j. Figure 7 displays the variation of $\bar{w}(L)$ with η obtained in the simulation of the electrodissolution of the electrode model according to Eq. (10) and using Eq. (9). $\bar{w}(L)$ is the saturation value of interface width, reached after time $T^*(L)$ when horizontal correlations of interface heights reach the system size L.[42] It appears normalized by the equivalent value corresponding to the perfect random dissolution, $\bar{w}_{\mathrm{RD}}(L)$, obtained from the simulation of the simplest reactive model: $M \xrightarrow{k} M^{z+}_{\mathrm{sol}} + ze^-$. Since all interface sites are in state M, the hypotheses of our interface model assure a homogeneous dissolution. Each set of points corresponds to a different set of kinetic parameters $\{k_{0,1}, k_{0,-1}, k_{0,2}, \alpha_1, \alpha_2\}$ (the solid lines will be discussed later).

The preferential dissolution mechanism induced by the spontaneous chemical heterogeneity lies beneath the results displayed in Fig. 7. This can be understood with the help of Fig. 8, which depicts the dependence on η of the ratio between the mean height of interface $\tilde{h}$ and the mean height of active dissolution sites in Eq. (10)—those cells in state $M(\mathrm{I})_{\mathrm{ads}}$—$\tilde{h}_1$. A correlation between the variation of surface roughness and that of $\tilde{h}/\tilde{h}_1$ emerges from the comparison with Fig. 7. When the chemical heterogeneity is negligible ($\tilde{h}/\tilde{h}_1 \to 1$), active dissolution sites are homogeneously distributed on the surface and roughness is the same to that of

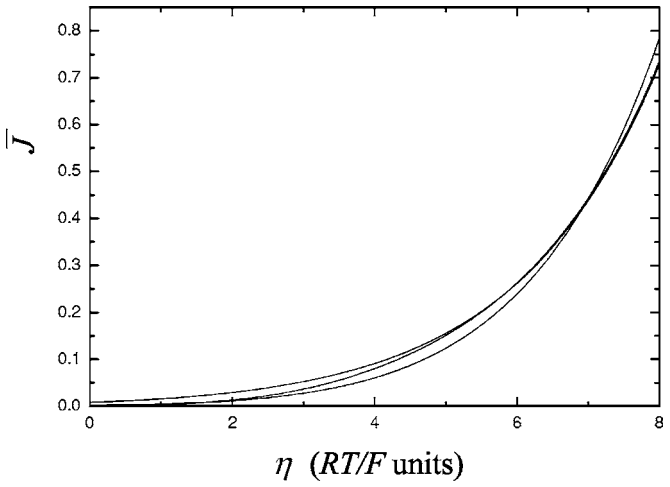

FIG. 9. Electrode polarization curve corresponding to each set of kinetic parameters of Fig. 7. Steady-state current density $\bar{J}$ has been calculated from Eq. (12). Values obtained from this macroscopic approach are quite similar to those obtained in the simulations.

the random dissolution model. The decrease in the $\tilde{h}/\tilde{h}_1$ ratio indicates the shift of the preferential dissolution sites toward higher positions on the interface; dissolution thus acts as a smoothing mechanism that diminishes $\bar{w}(L)$. It is also worth noting that for two of the three sets of kinetic parameters, the normalized roughness deviates from the expected random dissolution behavior even at open-circuit conditions (η=0), which means that chemical heterogeneity may take place at spontaneously evolving interfaces.

Values of parameters in Figs. 7 and 8 have been chosen to illustrate the fact that surface roughness can vary with the overpotential in completely different ways that are nonetheless not reflected in the steady-state polarization curve of the electrode. In Fig. 9, we show, for the three cases of Fig. 7, the variation with η of the steady-state current density $\bar{J}$, which is obtained from the charge balance across the interface:

$$\bar{J} = k_1(1 - \bar{\Theta}_1) + (k_2 - k_{-1})\bar{\Theta}_1. \tag{12}$$

$\bar{\Theta}_1$ is the surface coverage fraction of the adsorbed species $M(\mathrm{I})_{\mathrm{ads}}$ at steady state, obtained from the mass balance across the interface:

$$\frac{d}{dt}\Theta_1 = k_1(1 - \Theta_1) - (k_2 + k_{-1})\Theta_1. \tag{13}$$

In classical electrochemistry, the deduction of dissolution mechanisms and kinetics is based on mathematical models—as those in Eqs. (12) and (13)—that fit the experimental steady (polarization curve) and nonsteady (electrochemical impedance) responses of the electrode.[55] Since the polarization curves depicted in Fig. 9 are quite similar independently of the different kinetics simulated, it clearly appears that the simple steady-state experimental approach does not allow the full comprehension of interface kinetics. Non-steady-state techniques give deeper interface insights but, consistent with what is presented in the present work, the effect of surface relaxation on the experimental results is still a matter of solid discrepancies in the literature.[57] In this sense, taking advantage of the current facilities for roughness observation in all scales, Figs. 7 and 9 indicate that it would be interesting to incorporate this dynamic surface approach to the classical electrochemical models, which could contribute to those processes of mechanistic deduction. This would be theoretically feasible provided that one can mathematically establish the interplay between roughness and the physical and chemical processes that take part in the dissolution process, which is the aim of the next section.

B. Kinetic model for roughness

We can elaborate further on the relationship between roughness and the ratio $\tilde{h}/\tilde{h}_1$ by invoking the linear approximation discussed in the previous section and the connection of $\tilde{h}/\tilde{h}_1$ to its kinetic equivalent $\tilde{t}/\tilde{t}_1$, where $\tilde{t}_1$ is defined in Eq. (4) and $\tilde{t}$ is given by

$$\tilde{t} = \frac{\int_0^\infty [p_0(t) + p_1(t)]t dt}{\int_0^\infty [p_0(t) + p_1(t)]dt}, \tag{14}$$

with $p_0(t)$ and $p_1(t)$ as solutions to the differential system equivalent to Eq. (2) for model (10). To calculate the dependence of $\tilde{t}/\tilde{t}_1$ on the overpotential η, we can solve the equivalent differential system and integrate its solutions according to Eqs. (4) and (14). Instead of that, we shall adopt a much simpler strategy that will easily lead us to a simply analytic expression. For that purpose, we shall make use of another definition for $\bar{\Theta}_i$, obtained from the macroscopic equations,

$$\bar{\Theta}_i = \frac{\int_0^\infty p_i dt}{\int_0^\infty \sum_j p_j dt}, \tag{15}$$

and we shall consider the following algebraic relations between the mean times $\tilde{t}_0$ and $\tilde{t}_1$:

$$\tilde{t}_0 = \frac{1}{R_1} + \tilde{t}_1\left(\frac{R_{-1}}{R_2 + R_{-1}}\right),$$
$$\tilde{t}_1 = \tilde{t}_0 + \frac{1}{R_2 + R_{-1}}. \tag{16}$$

The first equation in Eq. (16) establishes that the mean time of state M is equal to the mean time corresponding to its oxidation, $1/R_1$, plus the mean time corresponding to the oxidized state $M(\mathrm{I})_{\mathrm{ads}}$ weighted by its relative probability of reduction back to state M. In the second equation, $\tilde{t}_1$ is equal to the mean time of its predecessor, $\tilde{t}_0$, plus the mean lifetime of state $M(\mathrm{I})_{\mathrm{ads}}$, which is given by the inverse of the sum of

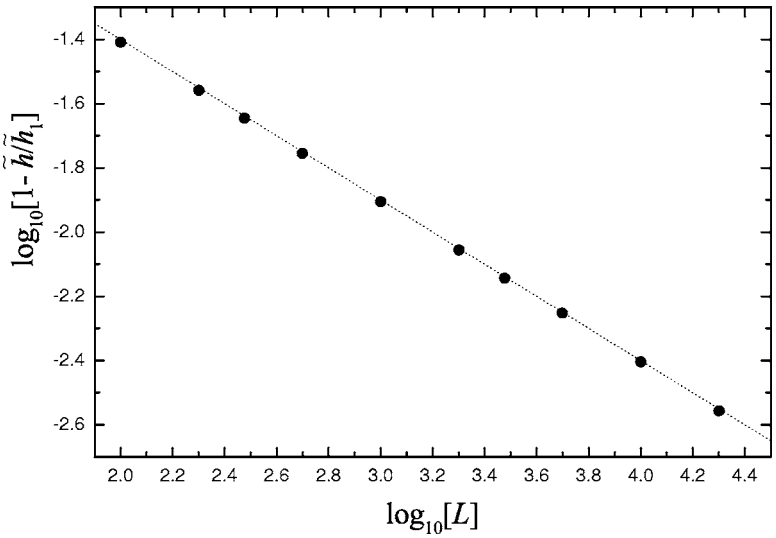

FIG. 10. Dependence of $1-\tilde{h}/\tilde{h}_1$ on L in base-10 logarithms for the kinetic case $R_1=R_2$ and $R_{-1}=0$. Each point is the average of n independent runs, with n decreasing from 5000 ($L=100$) up to 50 runs ($L=2\times10^4$). The dotted line with a slope of −0.5 has been plotted for comparison. The results correspond to the Von Neumann neighborhood.

the reaction probabilities that transform that state, $1/(R_2+R_{-1})$.

According to Eq. (15), Eq. (14) can be written as

$$\tilde{t}=\tilde{t}_0\bar{\Theta}_0+\tilde{t}_1\bar{\Theta}_1. \tag{17}$$

By solving the algebraic system in Eq. (16) and by substituting into Eq. (17) the values of $\tilde{t}_0,\tilde{t}_1$, $\bar{\Theta}_0=1-\bar{\Theta}_1$, and $\bar{\Theta}_1$ obtained from the stationary condition in Eq. (13) with the kinetic constants replaced by the corresponding transition probabilities, we obtain

$$\frac{\tilde{t}}{\tilde{t}_1}=\frac{R_1^2+(R_2+R_{-1})^2+R_1(R_2+2R_{-1})}{(R_1+R_2+R_{-1})^2}, \tag{18}$$

with the dependence on η through Eq. (9).

Variation of $\tilde{t}/\tilde{t}_1$ with η, obtained from Eq. (18), has been displayed in Fig. 7 in continuous lines for the three sets of kinetic parameters used in the simulations. This variation is quantitatively similar to the change of the steady interface roughness with the polarization of the electrode, sustaining the so-called linear approximation. Results show that $\tilde{t}/\tilde{t}_1$ can potentially represent a dimensionless analytic kinetic descriptor of the interface roughness.

C. Scaling behavior

We shall finish analyzing the influence of the system size L on the results presented in this work. Since chemical ordering essentially develops at microscopic scales, correlations between the chemical species will not be affected if L changes, whenever this value is larger than the correlations range. With respect to the height ordering, differences between the mean heights of the different species $(\tilde{h}_i-\tilde{h}_j)$ are also independent of the lattice size. However, the influence of scale on the chemical ordering manifests when considering the ratios between the mean heights. In Fig. 10, we show how $\tilde{h}/\tilde{h}_1$ varies with L in the kinetic case corresponding to the minimum value of roughness in Fig. 7 (obtained with $R_1\approx R_2$ and $R_{-1}\approx0$, and giving $\bar{\Theta}_1\approx0.5$). We see that $1-\tilde{h}/\tilde{h}_1$ decreases as a power law of the form

$$1-\tilde{h}/\tilde{h}_1\sim L^{-0.5}. \tag{19}$$

Since $\tilde{h}_1-\tilde{h}$ is independent of L, we obtain that $\tilde{h}_1$ scales with the system size as a power law of L with exponent of 0.5.

This value does not depend on the dissolution reactive mechanism considered in simulations or the values of kinetic parameters employed in the model. Actually, it is a consequence of the scaling behavior of dissolving solid surfaces under a surface reaction kinetic control. For those processes, it has been shown[43,49,53] that the interface is self-affine and its width scales with the time of evolution and system size in the following form, established by the dynamic scaling theory known as the Family-Vicsek scaling:[42]

$$w(L,t)\sim L^{\alpha}f\left(\frac{t}{L^{\alpha/\beta}}\right), \tag{20}$$

with $f(u)\sim$ const if $u\gg1$ and $f(u)\sim u^{\beta}$ if $u\ll1$. In the case of (1+1)D dissolution processes without surface diffusion,[43,53] values of the growth (β) and roughness (α) exponents approach those predicted by the two-dimensional Kardar-Parisi-Zhang equation, indicating that these processes belong to the same universality class as the Eden or the ballistic deposition models in surface growth. In fact, scaling analysis of interfaces obtained in simulations considering different reaction models and different kinetic regimes has shown the values $\beta\approx0.33$ and $\alpha\approx0.5$ in all cases, which are similar to the values of 1/3 and 1/2 predicted by the continuum theory. The scaling law $\bar{w}(L)\sim L^{0.5}$ and the self-affinity properties of interface assure that all height distances scale with the same power law, thus explaining the result in Eq. (19).

To conclude, we analyze the scaling behavior of the differences in roughness displayed in Fig. 7. If the origin of the preferential mechanism lies in the microscopic chemical ordering, we could expect that those differences are due to some type of intrinsic width w_{intr} that does not scale with the system size, and whose effect on the roughness scaling could be described by the following convolution approximation:[42]

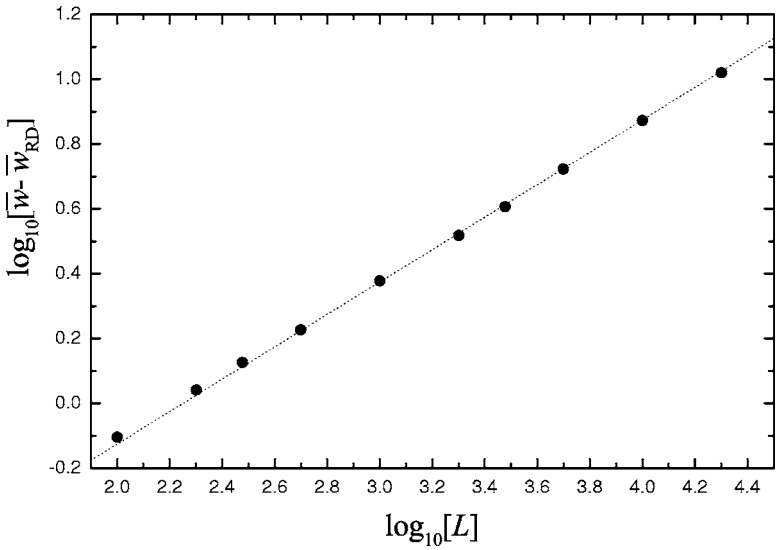

FIG. 11. Dependence of $\bar{w}(L)-\bar{w}_{\mathrm{RD}}(L)$ on L in base-10 logarithms for the kinetic case $R_1=R_2$ and $R_{-1}=0$. Each point is the average of n independent runs, with n decreasing from 5000 ($L=100$) up to 100 runs ($L=2\times10^4$). The dotted line with a slope of 0.5 has been plotted for comparison. The results correspond to the Von Neumann neighborhood.

$$w^2(L,t) = w^2_{\mathrm{RD}}(L,t) + w^2_{\mathrm{intr}}(t). \tag{21}$$

According to that argument, the interface width obtained from simulations of model (10) should converge to that of the random dissolution model for large enough systems. However, the results support the idea that differences persist in all scales, increasing in the form of a power law with the same exponent of 0.5. In Fig. 11, we show the scaling behavior of the difference between the roughness of the minimum point in Fig. 7 and that of the random dissolution model. It can be seen that this difference also scales in the form $\sim L^{0.5}$. Again, this holds for the whole set of points displayed in Fig. 7, so we can conclude that the behavior displayed in that figure is independent of the scale considered. Taking account of the good estimation obtained from the kinetic parameter $\tilde{t}/\tilde{t}_1$, we can finally write

$$\bar{w}(L,k) \approx \frac{\tilde{t}}{\tilde{t}_1}(k)\bar{w}_{\mathrm{RD}}(L), \tag{22}$$

where the symbol k stands for the kinetics of the process. Equation (22) suggests that the dependence of interface roughness on both the dissolution kinetics and the system size can be split into two terms: a first purely kinetic term, $\tilde{t}/\tilde{t}_1(k)$, given by Eq. (18) for model (10), which carries in an analytic way the influence of the electrochemical kinetics on roughness, and a second term, $\bar{w}_{\mathrm{RD}}(L)$, providing the characteristic roughness intrinsic to the stochastic nature of dissolution and dependent on L.

IV. DISCUSSION

A large class of uniform and localized corrosion processes involves several chemical and electrochemical reactive steps with the participation of metal atoms and chemical species from the solution. This set of elementary reactions constitutes the corrosion mechanism, which varies according to the type of metal and the electrolyte composition. In many cases, the mechanism includes adsorption-desorption processes leading to adsorbates, as in the dissolution of iron in acidic medium. The adsorption of anions may form compounds with the surface metallic sites, intermediate states, while some cations may be reduced, yielding simple adsorbates, as in the hydrogen evolution mechanism. In other cases, as dissolution in some basic or neutral solutions, the corrosion product may be adherent and only the presence of aggressive anions can induce its dissolution from the metal surface. In all of these cases, the existence of coupled interfacial reactions unavoidably establishes a time ordering in the reaction sequence.

The theoretical and computational analysis of a simple dissolution model has revealed a different mechanism of chemical ordering on nonequilibrium evolving metal-electrolyte interfaces: the time ordering of chemical species implicit to the reactive scheme is projected into the spatial dimension by the stochastic roughening of the metal surface. We have focused, in the explanation of the mechanism, on the general features of that chemical ordering, and its consequences on the interface dynamics. However, we have not displayed all possible scenarios that can be obtained by varying the reactive kinetics or the dissolution scheme. These scenarios can show long-ranged correlation—in contrast to the short-ranged correlations shown in Sec. II or even no ordering, i.e., homogeneous distribution of reactants. In any case, the chemical organization can be predicted analytically, at least in a qualitative way, from the mean-field macroscopic approach developed in Sec. II B.

The understanding of the processes that participate in the roughening of a metallic electrode is essential both theoretically and experimentally. It opens up the way for the establishment of the correct link between external parameters such as the applied electrical potential or the electrolyte composition and a technologically important aspect such as the surface topography. In my opinion, this work represents a contribution to that understanding. As we have shown, chemical ordering can favor or inhibit the development of roughness in function of these external parameters. It is important to notice that this effect scales with the system size, so it is observable in the macroscopic scales of the model. By working with a single scheme (10), we have focused on the influ-

ence of the applied potential. In this sense, the electrode response to variations of potential constitutes one of the major sources of experimental data to gather information about the electrochemical processes taking part at the interface. In this work, we have related analytically the roughness response of the electrode with the driven electrochemical kinetics. The results presented in this paper suggest that roughness, which can be measured in all scales with the aid of the modern nanoscopic imaging techniques, could represent, in the early future, an experimental parameter that provides information about the mechanism and kinetics of a given process.

ACKNOWLEDGMENTS

The author would like to thank Víctor Fairén for fruitful discussions and Ricardo P. Nogueira and Daniel Rodríguez-Pérez for their always certain remarks and comments about this work.

*Fax: (+34) 913987628. Email address: pcordoba@dfmf.uned.es

[1] I. Stengers and I. Prigogine, *Order Out of Chaos* (Heinemann, London, 1984).
[2] R. M. Ziff, E. Gulari, and Y. Barshad, Phys. Rev. Lett. **56**, 2553 (1986).
[3] D. Gupta and C. S. Hirtzel, Mol. Phys. **68**, 583 (1989).
[4] M. Silvergerg and A. Ben-Shaul, J. Chem. Phys. **87**, 3178 (1987); Surf. Sci. **214**, 43 (1989).
[5] B. Hellsing and V. P. Zhdanov, Chem. Phys. Lett. **147**, 613 (1988).
[6] O. M. Becker, M. Silverberg, and A. Ben-Shaul, Isr. J. Chem. **30**, 179 (1990).
[7] E. S. Hood, B. H. Toby, and W. H. Weinberg, Phys. Rev. Lett. **55**, 2437 (1985).
[8] O. M. Becker and A. Ben-Shaul, Phys. Rev. Lett. **61**, 2859 (1988).
[9] M. Polak and L. Rubinovich, Surf. Sci. Rep. **38**, 127 (2000).
[10] L. N. Gumen, E. P. Feldman, V. M. Yurchenko, T. N. Mel'nik, and A. A. Krokhin, Surf. Sci. **445**, 526 (2000).
[11] E. Christoffersen, P. Stoltze, and J. K. Nørskov, Surf. Sci. **505**, 200 (2002).
[12] V. P. Zhdanov, Surf. Sci. **500**, 966 (2002).
[13] B. Ben-Avraham and S. Havlin, *Diffusion and Reactions in Fractals and Disordered Systems* (Cambridge University Press, Cambridge, U.K., 2000).
[14] B. Bonnier, Phys. Rev. E **61**, 1270 (2000).
[15] F. Vikas, F. Baras, and G. Nicolis, Phys. Rev. E **66**, 036133 (2002).
[16] S. Habib, K. Lindenberg, G. Lythe, and C. Molina-París, J. Chem. Phys. **115**, 73 (2001).
[17] R. Kopelman, Science **241**, 1620 (1988).
[18] L. K. Gallos and P. Argyrakis, Phys. Rev. Lett. **92**, 138301 (2004).
[19] P. Córdoba-Torres, R. P. Nogueira, and V. Fairén, Phys. Rev. E **70**, 061108 (2004).
[20] U. W. Pohl, K. Pötschke, A. Schliwa, F. Guffarth, D. Bimberg, N. D. Zakharov, P. Werner, M. B. Lifshits, V. A. Shchukin, and D. E. Jesson, Phys. Rev. B **72**, 245332 (2005).
[21] D. Babonneau, F. Pailloux, J.-P. Eymery, M.-F. Denanot, Ph. Guérin, E. Fonda, and O. Lyon, Phys. Rev. B **71**, 035430 (2005).
[22] G. Capellini, M. De Seta, F. Evangelisti, V. A. Zinovyev, G. Vastola, F. Montalenti, and L. Miglio, Phys. Rev. Lett. **96**, 106102 (2006).
[23] R. A. Puglisi, G. Nicotra, S. Lombardo, C. Spinella, G. Ammendola, and C. Gerardi, Phys. Rev. B **71**, 125322 (2005).
[24] J. Stangl, V. Holý, and G. Bauer, Rev. Mod. Phys. **76**, 725 (2004).
[25] G. Oshanin and S. F. Burlatsky, Phys. Rev. E **67**, 016115 (2003).
[26] P. Argyrakis, S. F. Burlatsky, E. Clément and G. Oshanin, Phys. Rev. E **63**, 021110 (2001).
[27] M. Coppey, O. Bénichou, J. Klafter, M. Moreau, and G. Oshanin, Phys. Rev. E **69**, 036115 (2004).
[28] G. Oshanin, M. N. Popescu, and S. Dietrich, Phys. Rev. Lett. **93**, 020602 (2004).
[29] S. R. Shinde, Abhijit S. Ogale, S. B. Ogale, S. Aggarwal, V. Novikov, E. D. Williams, and R. Ramesh, Phys. Rev. B **64**, 035408 (2001); Abhijit S. Ogale, *ibid.* **64**, 035409 (2001).
[30] C. Stampfl, M. V. Ganduglia-Pirovano, K. Reuter, and M. Scheffler, Surf. Sci. **500**, 368 (2002).
[31] P. Córdoba-Torres, K. Bar-Eli, and V. Fairén, J. Electroanal. Chem. **571**, 189 (2004).
[32] J. Wang, A. J. Davenport, H. S. Isaacs, and B. M. Ocko, Science **255**, 1416 (1992).
[33] S. Manne, P. K. Hansma, J. Massie, V. B. Elings, and A. A. Gewirth, Science **251**, 307 (1991).
[34] C. L. Fu and K. M. Ho, Phys. Rev. Lett. **63**, 1617 (1989).
[35] K. J. Vetter, *Electrochemical Kinetics* (Academic, New York, 1967).
[36] O. M. Magnussen and M. R. Vogt, Phys. Rev. Lett. **85**, 357 (2000).
[37] M. G. Fernandes, R. M. Latanision, and P. C. Searson, Phys. Rev. B **47**, 11749 (1993).
[38] W. Allgaier and K. E. Heusler, J. Appl. Electrochem. **9**, 155 (1979).
[39] B. Folleher and K. E. Heusler, J. Electroanal. Chem. Interfacial Electrochem. **180**, 77 (1984).
[40] M. R. Vogt, A. Lachenwitzer, O. M. Magnussen, and R. J. Behm, Surf. Sci. **399**, 49 (1998).
[41] D. W. Suggs and A. J. Bard, J. Am. Chem. Soc. **116**, 10725 (1994).
[42] A. L. Barabási and H. E. Stanley, *Fractal Concepts in Surface Growth* (Cambridge University Press, New York, 1995).
[43] A. Hernández Creus, P. Carro, R. C. Salvarezza, and A. J. Arvia, J. Electrochem. Soc. **142**, 3806 (1995).
[44] M. E. Vela, G. Andreasen, R. C. Salvarezza, A. Hernández-Creus, and A. J. Arvia, Phys. Rev. B **53**, 10217 (1996).
[45] S. G. Aziz, M. E. Vela, G. Andreasen, R. C. Salvarezza, A. Hernández-Creus, and A. J. Arvia, Phys. Rev. B **56**, 4166 (1997).

[46] J. E. T. Andersen, G. Bech-Nielsen, P. Moeller, and J. C. Reeves, J. Appl. Electrochem. **26**, 161 (1996).
[47] M. E. Vela, G. Andreasen, S. G. Aziz, R. C. Salvarezza, and A. J. Arvia, Electrochim. Acta **43**, 3 (1998).
[48] A. Iwamoto, T. Yoshinobu, and H. Iwasaki, Phys. Rev. E **59**, 5133 (1999).
[49] A. Hernández Creus, P. Carro, R. C. Salvarezza, and A. J. Arvia, Langmuir **13**, 833 (1997).
[50] M. Saitou, A. Makabe, and T. Tomoyose, J. Chem. Phys. **113**, 2397 (2000).
[51] H. Martín, P. Carro, A. Hernández Creus, J. Morales, G. Fernández, P. Esparza, S. González, R. C. Salvarezza, and A. J. Arvia, J. Phys. Chem. B **104**, 8229 (2000).
[52] J. R. LaGraff and A. A. Gewirth, Surf. Sci. **326**, L461 (1995).
[53] B. A. Mello, A. S. Chaves, and F. A. Oliveira, Phys. Rev. E **63**, 041113 (2001).
[54] G. Poupard and G. Zumofen, J. Phys. A **25**, L1173 (1992).
[55] M. Keddam, O. R. Mattos, and H. Takenouti, J. Electrochem. Soc. **128**, 257 (1981); **128**, 266 (1981).
[56] J. O'M. Bockris, D. Drazic, and A. R. Despic, Electrochim. Acta **4**, 326 (1961).
[57] L. M. Gassa, J. N. Lambi, A. E. Bolzán, and A. J. Arvia, J. Electroanal. Chem. **527**, 71 (2002).